Triggering Processes in Rock Fracture

Jörn Davidsen,[1,2,*] Grzegorz Kwiatek,[2] Elli-Maria Charalampidou,[3] Thomas Goebel,[4] Sergei Stanchits,[5] Marc Rück,[2] and Georg Dresen[2,6]

[1]Complexity Science Group, Department of Physics and Astronomy, University of Calgary, Calgary, Alberta T2N 1N4, Canada
[2]GFZ German Research Centre for Geosciences, Section III.2: Geomechanics and Rheology, 14473 Potsdam, Germany
[3]Heriot–Watt University, Institute of Petroleum Engineering, Edinburgh EH14 4AS, United Kingdom
[4]University of California, Santa Cruz, Earth & Planetary Sciences, Santa Cruz, California 95064, USA
[5]Schlumberger Research, Salt Lake City, Utah 84104, USA
[6]University of Potsdam, 14469 Potsdam, Germany

(Received 4 December 2015; revised manuscript received 15 June 2017; published 8 August 2017)

We study triggering processes in triaxial compression experiments under a constant displacement rate on sandstone and granite samples using spatially located acoustic emission events and their focal mechanisms. We present strong evidence that event-event triggering plays an important role in the presence of large-scale or macrocopic imperfections, while such triggering is basically absent if no significant imperfections are present. In the former case, we recover all established empirical relations of aftershock seismicity including the Gutenberg-Richter relation, a modified version of the Omori-Utsu relation and the productivity relation—despite the fact that the activity is dominated by compaction-type events and triggering cascades have a swarmlike topology. For the Gutenberg-Richter relations, we find that the b value is smaller for triggered events compared to background events. Moreover, we show that triggered acoustic emission events have a focal mechanism much more similar to their associated trigger than expected by chance.

DOI: 10.1103/PhysRevLett.119.068501

Introduction.—One of the hallmarks of our understanding of seismicity in nature is the importance of triggering processes, which makes the forecasting of seismic activity feasible [1–3]. These triggering processes by which one earthquake induces (dynamic or static) stress changes leading to potentially multiple other earthquakes [4–7] are at the core relaxation processes [8]. A specific example of triggering are aftershocks following a large earthquake [9–13]. These aftershocks obey certain empirical laws that characterize, for example, their spatio-temporal distribution, as is the case for the Omori-Utsu (OU) relation [14]. This relation gives the local rate of triggered activity following a main shock: after a time t, the rate is $r(t) = [K/(t+c)^p]$ with usually $p \approx 1$. Such an empirical law should arise from the underlying microscopic dynamics of the involved physical processes, but the exact connection remains to be established. Simple explanations have been proposed, but their general applicability is unclear [15]. Many explanations involve the picture of an earthquake as a purely frictional sliding event [16,17]. In the lab, earthquakelike stick-slip sliding on rough granite surfaces produces acoustic emission (AE) events—related to the nucleation and growth of microcracks corresponding to mini earthquakes [18,19] often considered a special type of crackling noise [20,21]—that show statistical behavior similar to tectonic seismicity. This includes Omori-type aftershock decay as well as Gutenberg-Richter (GR) frequency-magnitude distributions [22]. Recent uniaxial compression experiments on different materials have shown that the OU relation and most empirical laws of seismicity can also be observed for AE events *before* the failure point [23,24]. This suggests that fracture phenomena can also give rise to triggering associated with aftershocks. The observation of triggering in uniaxial tests is surprising because triggering is absent during triaxial fracture experiments on homogeneous samples such as sandstone, for which AE activity increases as a nonhomogeneous Poisson process [25]. Similarly, numerical simulations of a model of sedimentary rocks with time-independent rheology subject to uniaxial compression do not show such triggering behavior [26]. More importantly, Refs. [25,26] both provide clear examples that spatial localization and an increase in activity rates do *not* necessarily imply triggering behavior associated with aftershocks. Another uniaxial compression experiment seems to suggest time-dependent deviations from the OU relation [27], while other studies suggest that the OU relation is a general or even universal signature of relaxation processes in rock fracture independent of the specific perturbation source [8,28].

To clarify the occurrence and properties of triggering processes in rock fracture, we study here *triaxial* compression experiments under a constant displacement rate on sandstone and granite samples, using *spatially located* AE events and their *focal mechanisms*. This has the advantage that (i) we realize conditions that are closer to those relevant for earthquakes, (ii) we can use an established methodology to identify triggering relationships, and (iii) we can analyze the involved source parameters. We find that pronounced event-event triggering is only observable in the presence of large-scale imperfections such as a notch or inclusion in the sample. Triggering cascades tend to propagate away from

the imperfections, and large cascades have a more swarmlike topology as observed for earthquakes in areas of high heat flow [29]. The triggered events typically have a focal mechanism more similar to their trigger than expected by chance, and they follow a GR distribution with a significantly lower b value than observed for background events (events without a trigger)—both features have also been reported for earthquakes [10,30]. Moreover, the triggering rates can be well approximated by a power law with an exponent $p \approx 0.75$ similar to the OU relation but with a faster decay at later times. This behavior is independent of the magnitude of the trigger and is captured by a universal scaling function, reminiscent of critical phenomena [31].

Experiments.—Triaxial compression experiments ($\sigma_2 = \sigma_3 < \sigma_1$) were performed on sandstone and granite samples of 4–5 cm in diameter and 10–11 cm in height at a constant axial displacement rate $\dot{u} = 20\ \mu\mathrm{m/min}$. The high compressive loading stresses and specific rock properties favored the formation of compaction bands in Bleuerswiller sandstone (Vo3, porosity 24%, 80 MPa confining pressure, wet, 10 MPa pore pressure [32]) and Bentheim sandstone (Be7a, porosity 22%, 160 MPa confining pressure, dry [33]) and the formation of localized fracture zones in two Westerly granite samples (Wgrn07, Wgp01, porosity $\approx 0.15\% - 0.7\%$, 75 MPa confining pressure, dry [34,35]). No large-scale imperfections were identified in samples Vo3 and Wgp01. The Be7a sample had a 5 mm-deep saw-cut notch of 0.8 mm in height at its midlength, oriented at 90° to the samples loading axis [33,36]. A natural high density inclusion (max size of 1×0.9 cm) was located near the notch [33], as revealed by x-ray computed tomography imaging. Large-scale imperfections in the Wgrn07 sample were introduced by two 15 mm deep saw-cut notches inclined at 30° to the loading axis [34,35]).

We analyzed AE data during loading at a constant displacement rate before peak strength [37–39]. We performed a full moment tensor (FMT) inversion of AE data using first-motion P-wave amplitudes [40,41]. For selected pairs of AE events, we used the FMT solutions to calculate the 3D rotation angles δ between their P (pressure) and T (tension) axes directions [42].

Methodology.—To establish the presence or absence of triggering, we first follow an approach based on interevent times and the interevent time ratio R that has been successfully used in the context of earthquakes [5]. R_i is defined as $R_i = \Delta t_{i+1}/(\Delta t_i + \Delta t_{i+1})$ for all $1 < i < N$, where Δt_i is the time interval between event i and event $i-1$. The probability density function (PDF) is denoted by $p(R)$. For a Poisson process with no triggering, $p(R)$ is uniformly distributed between 0 and 1. A significant peak at $R = 0$ indicates triggering, similar to the behavior of related measures [43]. A peak at $R = 1$ indicates quiescence or anticlustering such that long interevent intervals tend to follow short interevent intervals. As large events are expected to trigger other events more frequently according to the productivity relation [10,44], the peak at 0 should become more pronounced if $p(R)$ is conditioned on magnitude. To minimize the effect of overlapping triggering sequences, one can condition on the magnitude difference such that only events that are preceded by a smaller one are considered.

The above analysis of the interevent time ratio is purely local in time. To take into account that triggering can take place over extended spatial and temporal scales involving multiple events and to identify triggering relations between AE events, we define triggered events (aftershocks) using the established methodology described in Refs. [10–12,45,46]. The basic idea is to look for violations of the null hypothesis that events occur randomly with a rate given by the GR relation. For a given event j, this can be quantified by $n_j^* = \min_{i<j}\{(r_{ij})^{D_f} t_{ij} \times 10^{-bm_i}\}$, where r_{ij} and t_{ij} are the spatial and temporal distances between the events, respectively. D_f is the (fractal) spatial dimension of the observed activity. Triggered events are those for which n^* is very low. The corresponding threshold value can be established by considering the distribution of the observed values of n^* split into a spatial and temporal part

$$\tau_j^* = t_j^* \times 10^{-bm_i^*/2}, \qquad l_j^* = (r_j^*)^{D_f} \times 10^{-bm_i^*/2}. \quad (1)$$

In the absence of triggering, the distribution is unimodal and typically indistinguishable from the distribution of randomized versions of the AE catalog where the time, location, and magnitudes are shuffled independently. These randomized versions also allow one to establish a suitable threshold value for n^*.

To quantify the topological structure of the triggering cascades, we use the concept of vertex depth—the minimal number d of links that connects a given triggered event to the tree root (the first event in a given triggering cascade) [29]. A useful scalar measure suitable for the following analysis is the average leaf depth $\langle d \rangle_f$—the vertex depth d averaged over the leaves of a given tree or triggering cascade (events that do not trigger themselves). A high $\langle d \rangle_f$ indicates a swarmlike activity, while a low $\langle d \rangle_f$ indicates a burstlike activity [29].

Results.—The presence of triggering is evident for the samples with large-scale imperfections (samples Be7a and Wgrn07) from Figs. 1 and 2. For the interevent time ratio, $p(R)$ shows significant deviations from the uniform distribution for the smallest and largest R, indicating clustering and anticlustering of events, respectively. The clustering dominates if one conditions on larger magnitudes or on larger magnitude differences as expected in the presence of triggering. The anticlustering might be related to the overall subcritical dynamics: triggering periods (local relaxation) are simply separated by longer time intervals due to the slow loading (global driving). The latter is similar to findings in [26]. In agreement with the behavior of $p(R)$ at small R, the density plots of the set $\{n_j^*\}$ (see

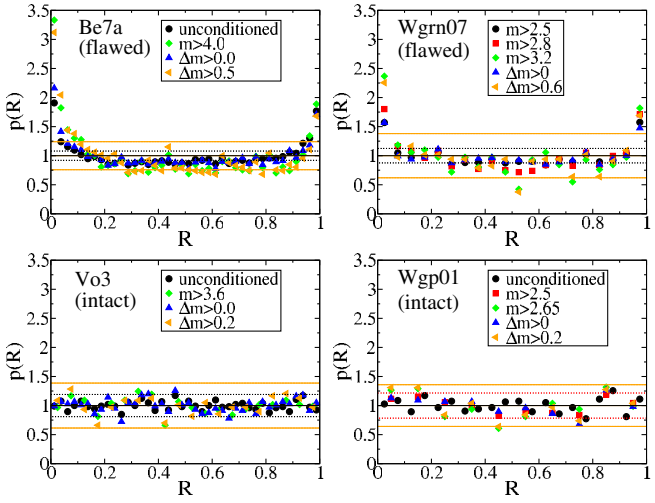

FIG. 1. PDF of the interevent time ratio R for different conditions on the magnitudes of the events evaluated for the different experiments. In all panels, the thick solid and dotted lines correspond to the 95% confidence intervals of a uniform distribution (based on Poissonian errors) for the largest Δm threshold ($\Delta m = m_{i+1} - m_i$) and the smallest m threshold (or the unconditioned case as indicated by color), respectively. These typically correspond to the largest and smallest uncertainties of all data sets shown in a panel.

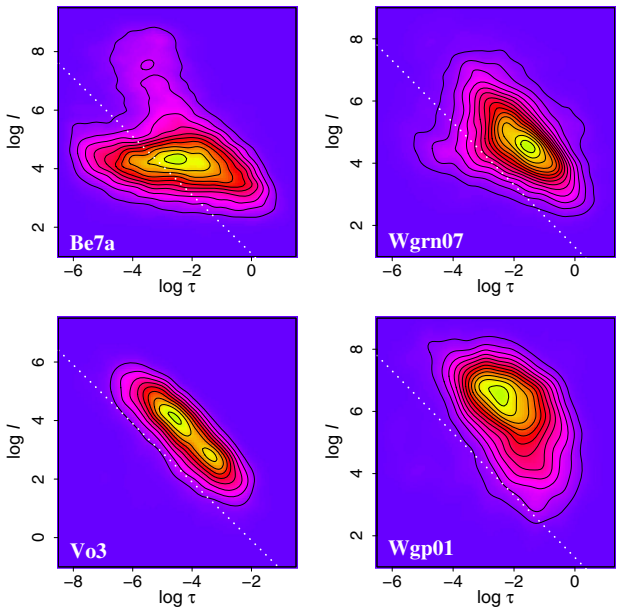

FIG. 2. Density plots of the set $\{n_j^* = \tau_i l_i\}$ for experiments with and without large scale imperfections (using $D_f = 2.3$ and the respective b values [see, e.g., Fig. 3)], represented in $\log\tau - \log l$ space as defined in Eq. (1). Data are denser in yellow and red regions and tend to zero density in blue regions. Time is measured in seconds, distances in millimeters. The straight lines (obtained from shuffled catalogs, Fig. S1 [37]) separate the two different populations of triggered events (below the line) and background events (above the line).

Fig. 2) also show that significant triggering is present. This is the first indication that triggering is associated with the presence of these imperfections. This is strongly supported by the samples without large-scale imperfections (samples Vo3 and Wgp01) as follows from Fig. 1. $p(R)$ shows no significant signs of triggering even if one conditions on larger magnitudes or on larger magnitude differences. Similarly, the density plots of the set $\{n_j^*\}$ (see Fig. 2) indicate that triggering is absent. This implies that the suggested mechanisms for triggering and the OU relation in damage mechanics—viscoelastic effects [47–49] or a broad distribution of characteristic times [15,50]—do not play an important role in the fracture of our intact samples, even close to failure (Figs. S2, S3 [37]).

To analyze the properties of the underlying triggering processes, we focus in the following on the triggered events (or aftershocks) for sample Be7a as defined in Fig. 2. The results for sample Wgrn07 (not shown) are consistent with those for sample Be7a. The role of the large-scale imperfections can be further established by considering the distance of the triggered events from a given imperfection. Figure 3(a) shows that triggering cascades tend to propagate away from the imperfection, consistent with process zone models [51–53]. Figure 3(b) shows that the topological structure of triggering cascades is characterized by an increase of $\langle d \rangle_f$ with increasing size and that $\langle d \rangle_f > 5$ for the largest triggering cascades. By definition, such high

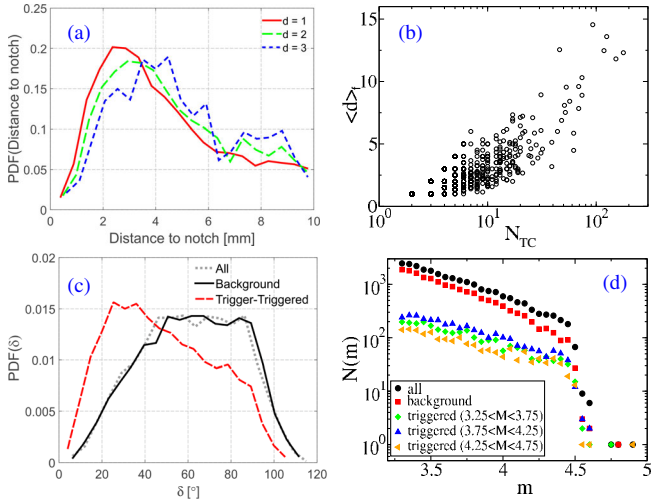

FIG. 3. Sample Be7a: (a) distribution of distances of triggered events from a large-scale imperfection (notch) for different vertex depths d in the triggering cascades. (b) Scatter plot of the average leaf depth $\langle d \rangle_f$ as a function of the number of events in the triggering cascade N_{TC}. (c) Distribution of rotation angles δ between the trigger and triggered event and for randomly selected pairs (background events only and all events, respectively). (d) Frequency-magnitude distribution for different AE events. M is the magnitude of the trigger (main shock). The estimated b values are 1.08 ± 0.08 (background events) and 0.75 ± 0.1 (triggered events).

values indicate that the cascades tend to follow a swarmlike structure and that the triggering process does not obey a simple branching process as often assumed [29]. Another feature of the underlying triggering process is that the distribution of 3D rotation angles δ between the trigger and triggered event is typically smaller than for random events, see Fig. 3(c). Rotation angles between 20° and 30° indicate highly similar focal mechanisms, consistent with triggering due to static stress changes [54].

Figure 3(d) shows that triggered events have a smaller b value than background events, independent of the magnitude of their trigger (main shock). This is consistent with the picture that the b value depends on the differential stress [55,56] as triggering should preferentially occur in areas that are closer to failure during prepeak loading. Nevertheless, the overall b values are similar to those observed in a variety of different AE experiments [19,23,24] such that b values alone are not generally indicative of the presence or absence of triggering.

The triggering rates as a function of time are shown in Fig. 4. Not only are there no significant variations over the duration of the experiment, but also under suitable rescaling with respect to the magnitude of the trigger (main shock), the functional behavior is well approximated by a universal scaling function. This follows from the data collapse in the lower inset of Fig. 4. The scaling function exhibits two different regimes. For smaller arguments, it decays as a power law with an exponent ≈0.75 [corresponding to the p value in the OU relation and consistent with the interevent time distribution for small times [57] (not shown)], which is similar to what has been observed in other AE experiments [23,24]. For larger arguments, we find a steeper power-law-like decay with an exponent of about 1.75. Note that the Kolmogorov-Smirnov test rejects the hypothesis that this decay is exponential at a confidence level higher than 99.99%, ruling out a superposition of characteristic times as the explanation for the observed behavior [15,50]. To our knowledge, this second power-law regime has not been observed in AE experiments before, which is likely a consequence of a lack of spatial information, which can make aftershock identification problematic in those cases [58]. While this behavior deviates from the classic OU relation, a similar behavior, albeit with slightly different exponents, has also been observed for tectonic seismicity [10,12]. Because of the data collapse under suitable rescaling (lower inset, Fig. 4), integrating the triggering rates over time gives rise to a productivity relation for the number of events triggered by a main shock of magnitude M, $N(M) \propto 10^{\alpha M}$ (upper inset Fig. 4), *independent* of the scaling function. In particular, $\alpha \approx 1.05$, which is simply the sum of the two exponents used for rescaling. This value is statistically indistinguishable from the result of the direct analysis of $N(M)$. Statistically identical exponents p and α are observed for sample Wgrn07. Other AE experiments have found $\alpha \approx 0.6$ [23,24], which could indicate nonuniversality [58].

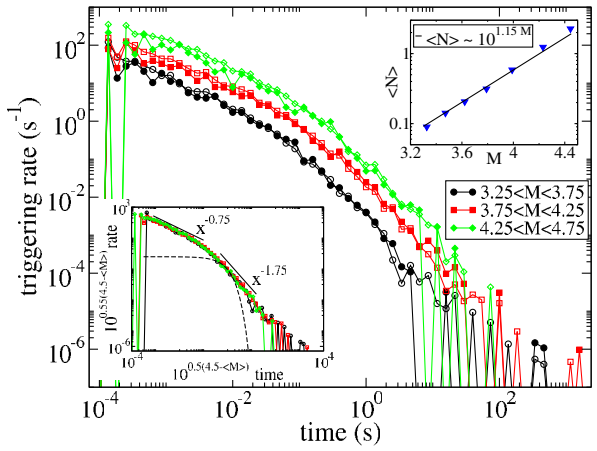

FIG. 4. Sample Be7a: triggering rate as a function of time averaged over different magnitude ranges of the trigger (main shock). Solid symbols correspond to a shorter subcatalog containing only about the first third of events. Lower inset: rates rescaled according to the magnitude of the trigger. An exponential (dashed line) is shown for comparison. Upper inset: productivity relation giving the average number of events triggered as a function of the trigger magnitude.

Discussion & Conclusions.—Our results suggest that triggering is generally detectable in the presence of macroscopic imperfections but remains undetectable or absent in experiments on homogeneous samples during prepeak loading. Our analysis of other experimental data over a wide range of rock types and under different loading conditions [19,35] confirms this. Our findings are consistent with the (direct or indirect) observation of triggering in other AE experiments. In Ref. [28], the sample exhibited a very complicated heterogeneous geometry. In Refs. [23,24], the sample sizes were much smaller than what we consider here and exhibited multifragmentation providing effective large-scale imperfections. It is important to realize though that we cannot fully rule out the presence of triggering in the absence of large-scale imperfections. It is possible that, in this case, the magnitudes of the triggered events just tend to be so small that they are below the magnitude of completeness in our experiments. In any case, the amount of triggered events and its relative contribution to the overall AE activity is certainly smaller in the absence of large-scale imperfections. A similar situation could apply to the case of micro-, nano-, and picoseismicity induced by mining as well as by long-term fluid injection where triggering also plays a smaller role [59].

The importance of large-scale imperfections for the occurrence of triggering is consistent with the picture that the local stress intensity, rather than the stress measured on the sample boundary, controls the susceptibility to triggering [60]. Since it is known that the interaction between a macroscopic crack and microcracks (AE events) leads to increased local stress fluctuations [61], our findings indicate

that such fluctuations are necessary for event-event triggering. This naturally explains the absence of triggering in intact samples even close to failure when the AE activity is localized (Figs. S2 and S3 [37] and Refs. [25,26]) but no macrocrack has formed yet. The importance of the interaction between large-scale imperfections and microcracks is conceptually consistent with process zone models [51–53]. Further support for this consistency comes from our direct observation that triggering cascades tend to propagate away from the imperfections. It is important to note though that there is no study so far that would relate the formation of a process zone to interactions at the scale of individual events. If established, such a relation should give rise to the OU relation in the triggering process during subcritical crack growth and provide a microscopic *event-based* explanation. Given that the failure of intact samples with localization but without triggering is also consistent with process zone models [25,62], our work highlights the need for microscopic process zone models that take the dynamics of the internal microscopic event-based stress redistribution directly into account.

Finally, our results also show that the productivity relation and an associated scale-invariant OU relation are not limited to frictional processes but also arise in compaction band formation as well as in fracture zone formation before the failure point is reached. Pore collapse and grain fragmentation are the main mechanisms associated with compaction band formation [63,64], and compaction-type events also dominate in shear banding [63] as well as in fracture zone formation (the polarity and focal mechanism analysis in Table S2 [37] gives 68% compaction-type events for sample Wgrn07 and even higher values for trigger and triggered events). Hence, our work proves conclusively that the occurrence of these empirical laws extends well beyond purely frictional sliding events, with potential applications in other types of crackling noise as well [65–70].

J. D. was financially supported by the Alexander von Humboldt-Foundation. J. D. would like to thank the GFZ for its hospitality and S. Hainzl for helpful discussions.

*davidsen@phas.ucalgary.ca

[1] D. Schorlemmer, J. D. Zechar, M. J. Werner, E. H. Field, D. D. Jackson, T. H. Jordan, and RELM Working Grp, Pure Appl. Geophys. **167**, 859 (2010).
[2] T. H. Jordan, Y. T. Chen, P. Gasparini, R. Madariaga, I. Main, W. Marzocchi, G. Papadopoulos, G. Sobolev, K. Yamaoka, and J. Zschau, Ann. Geophys. **54**, 319 (2011).
[3] K. F. Tiampo and R. Shcherbakov, Tectonophysics **522–523**, 89 (2012).
[4] E. E. Brodsky, Geophys. Res. Lett. **33**, L15313 (2006).
[5] N. J. van der Elst and E. E. Brodsky, J. Geophys. Res. **115**, B07311 (2010).
[6] N. J. van Der Elst, H. M. Savage, K. M. Keranen, and G. A. Abers, Science **341**, 164 (2013).
[7] S. Hainzl, J. Moradpour, and J. Davidsen, Geophys. Res. Lett. **41**, 8818 (2014).
[8] V. B. Smirnov and A. V. Ponomarev, Phys. Solid Earth **40**, 807 (2004).
[9] S. E. Hough and L. M. Jones, EOS, Trans. Am. Geophys. Union **78**, 505 (1997).
[10] C. Gu, A. Y. Schumann, M. Baiesi, and J. Davidsen, J. Geophys. Res. Solid Earth **118**, 4278 (2013).
[11] I. Zaliapin and Y. Ben-Zion, J. Geophys. Res. **118**, 2847 (2013).
[12] J. Moradpour, S. Hainzl, and J. Davidsen, J. Geophys. Res. **119**, 5518 (2014).
[13] J. Davidsen, C. Gu, and M. Baiesi, Geophys. J. Int. **201**, 965 (2015).
[14] T. Utsu, Y. Ogata, and R. S. Matsu'ura, J. Phys. Earth **43**, 1 (1995).
[15] C. H. Scholz, Bull. Seismol. Soc. Am. **58**, 1117 (1968).
[16] J. H. Dietrich, in *Earthquake Seismology*, edited by H. Kanamori Treatise on Geophysics Vol. 4 (Elsevier, Amsterdam, 2007), p. 107.
[17] S. Hainzl and D. Marsan, J. Geophys. Res. **113**, B10309 (2008).
[18] D. Lockner, Int. J. Rock Mech. Min. Sci. Geomech. Abstr. **30**, 883 (1993).
[19] J. Davidsen, S. Stanchits, and G. Dresen, Phys. Rev. Lett. **98**, 125502 (2007).
[20] J. P. Sethna, K. A. Dahmen, and C. R. Myers, Nature (London) **410**, 242 (2001).
[21] L. Laurson, X. Illa, S. Santucci, K. T. Tallakstad, K. J. Måløy, and M. J. Alava, Nat. Commun. **4**, 2927 (2013).
[22] T. H. W. Goebel, C. G. Sammis, T. W. Becker, G. Dresen, and D. Schorlemmer, Pure Appl. Geophys. **172**, 2247 (2015).
[23] J. Baró, Á. Corral, X. Illa, A. Planes, E. K. H. Salje, W. Schranz, D. E. Soto-Parra, and E. Vives, Phys. Rev. Lett. **110**, 088702 (2013).
[24] G. F. Nataf, P. O. Castillo-Villa, J. Baró, X. Illa, E. Vives, A. Planes, and E. K. H. Salje, Phys. Rev. E **90**, 022405 (2014).
[25] S. Lennartz-Sassinek, I. G. Main, M. Zaiser, and C. C. Graham, Phys. Rev. E **90**, 052401 (2014).
[26] F. Kun, I. Varga, S. Lennartz-Sassinek, and I. G. Main, Phys. Rev. Lett. **112**, 065501 (2014).
[27] T. Hirata, J. Geophys. Res. **92**, 6215 (1987).
[28] H. V. Ribeiro, L. S. Costa, L. G. A. Alves, P. A. Santoro, S. Picoli, E. K. Lenzi, and R. S. Mendes, Phys. Rev. Lett. **115**, 025503 (2015).
[29] I. Zaliapin and Y. Ben-Zion, J. Geophys. Res. **118**, 2865 (2013).
[30] K. Wong and F. P. Schoenberg, Bull. Seismol. Soc. Am. **99**, 3402 (2009).
[31] K. Christensen and N. R. Moloney, *Complexity and Criticality* (Imperial College Press, London, UK, 2005).
[32] J. Fortin, S. Stanchits, G. Dresen, and Y. Gueguen, Pure Appl. Geophys. **166**, 823 (2009).
[33] E. M. Charalampidou, G. Kwiatek, S. Stanchits, and G. Dresen, in *Proceedings of 10th Conference on Rock Physics and Rock Mechanics, Aussois, France* (2014). https://euroconf2014.sciencesconf.org/resource/page/id/11.
[34] T. H. W. Goebel, T. W. Becker, D. Schorlemmer, S. Stanchits, C. G. Sammis, E. Rybacki, and G. Dresen, J. Geophys. Res. **117**, B03310 (2012).

[35] T. H. W. Goebel, T. W. Becker, C. G. Sammis, G. Dresen, and D. Schorlemmer, Geophys. J. Int. **197**, 1705 (2014).
[36] G. Kwiatek, E.-M. Charalampidou, and G. Dresen, Int. J. Rock Mech. Min. Sci. Geomech. Abstr. **65**, 153 (2014).
[37] See Supplemental Material at http://link.aps.org/supplemental/10.1103/PhysRevLett.119.068501 for more information.
[38] S. Stanchits, S. Vinciguerra, and G. Dresen, Pure Appl. Geophys. **163**, 975 (2006).
[39] E.-M. Charalampidou, S. Stanchits, G. Kwiatek, and G. Dresen, Eur. J. Environ. Civ. En. **19**, 564 (2015).
[40] G. Kwiatek, T. H. W. Goebel, and G. Dresen, Geophys. Res. Lett., **41**, 5838 (2014).
[41] G. Kwiatek, P. Martínez-Garzón, and M. Bohnhoff, Seismol. Res. Lett. **87**, 964 (2016).
[42] Y. Y. Kagan, Geophys. J. Int. **171**, 411 (2007).
[43] J. Baró, J.-M. Martín-Olalla, F. J. Romero, M. C. Gallardo, E. K. H. Salje, E. Vives, and A. Planes, J. Phys. Condens. Matter **26**, 125401 (2014).
[44] A. Schmid and J.-R. Grasso, J. Geophys. Res. Solid Earth **117**, B07302 (2012).
[45] M. Baiesi and M. Paczuski, Phys. Rev. E **69**, 066106 (2004).
[46] I. Zaliapin, A. Gabrielov, V. Keilis-Borok, and H. Wong, Phys. Rev. Lett. **101**, 018501 (2008).
[47] K. Z. Nanjo, D. L. Turcotte, and R. Shcherbakov, J. Geophys. Res. Solid Earth **110**, B07403 (2005).
[48] Y. Ben-Zion, Rev. Geophys. **46**, RG4006 (2008).
[49] X. Zhang and R. Shcherbakov, Sci. Rep. **6**, 36668 (2016).
[50] C. Narteau, P. Shebalin, and M. Holschneider, J. Geophys. Res. **107**, 2359 (2002).
[51] D. Dugdale, J. Mech. Phys. Solids **8**, 100 (1960).
[52] G. I. Barenblatt, Adv. Appl. Mech. **7**, 55 (1962).
[53] A. Zang, F. C. Wagner, S. Stanchits, C. Janssen, and G. Dresen, J. Geophys. Res. **105**, 23651 (2000).
[54] D. E. Smith, J. H. Dietrich, and J. H. Dieterich, Pure Appl. Geophys. **167**, 1067 (2010).
[55] T. H. W. Goebel, D. Schorlemmer, T. W. Becker, G. Dresen, and C. G. Sammis, Geophys. Res. Lett. **40**, 2049 (2013).
[56] C. H. Scholz, Geophys. Res. Lett. **42**, 1399 (2015).
[57] R. Shcherbakov, G. Yakovlev, D. L. Turcotte, and J. B. Rundle, Phys. Rev. Lett. **95**, 218501 (2005).
[58] J. Báro and J. Davidsen, Euro. Phys. J. ST, (to be published).
[59] J. Davidsen and G. Kwiatek, Phys. Rev. Lett. **110**, 068501 (2013).
[60] P. G. Meredith and B. K. Atkinson, Geophys. J. R. Astron. Soc. **75**, 1 (1983).
[61] M. Kachanov, Adv. Appl. Mech. **30**, 259 (1994).
[62] Z. Reches and D. A. Lockner, J. Geophys. Res. **99**, 18159 (1994).
[63] E. Charalampidou, S. Hall, S. Stanchits, H. Lewis, and G. Viggiani, Tectonophysics **503**, 8 (2011).
[64] E. M. Charalampidou, S. A. Hall, S. Stanchits, G. Viggiani, and H. Lewis, Int. J. Rock Mech. Min. Sci. Geomech. Abstr. **67**, 240 (2014).
[65] J. Rosti, J. Koivisto, P. Traversa, X. Illa, J. R. Grasso, and M. J. Alava, Int. J. Fract. **151**, 281 (2008).
[66] A. Tantot, S. Santucci, O. Ramos, S. Deschanel, M.-A. A. Verdier, E. Mony, Y. Wei, S. Ciliberto, L. Vanel, and P. C. F. Di Stefano, Phys. Rev. Lett. **111**, 154301 (2013).
[67] K. T. Tallakstad, R. Toussaint, S. Santucci, and K. J. Måløy, Phys. Rev. Lett. **110**, 145501 (2013).
[68] M. Stojanova, S. Santucci, L. Vanel, and O. Ramos, Phys. Rev. Lett. **112**, 115502 (2014).
[69] J. T. Uhl *et al.*, Sci. Rep. **5**, 16493 (2015).
[70] T. Mäkinen, A. Miksic, M. Ovaska, and M. J. Alava, Phys. Rev. Lett. **115**, 055501 (2015).